Recursive Carrier Interferometry Aided High Data Rate OFDM Systems with PAPR Suppression, Phase Noise Rejection and Carrier Frequency Offsets Compensation

Huaiyin Lu[1], Lin Zhang[1*], *Member, IEEE*, Xianyu Chen[1], and Zhiqiang Wu[23], *Senior Member, IEEE*
Sun Yat-sen University[1], Tibet University[2], Wright State University[3]

***Abstract*—In this paper, we propose two groups of recursive codes, namely the Hadamard recursive carrier interferometry (HRCI) codes and diagonal recursive carrier interferometry (DRCI) codes, to simultaneously reduce the peak to average power ratio (PAPR) and suppress the phase noises and residual carrier frequency offset (RCFO) for high speed orthogonal frequency division multiplexing (OFDM) systems. We exploit the recursion property of the Hadamard and diagonal matrix to constitute the proposed HRCI code and DRCI code using the carrier interferometry (CI) code to spread the OFDM symbols in the frequency domain. Then, we prove that both HRCI and DRCI generation matrices keep their invertibility during the recursions. As a direct result of the new code design, the phase intervals are enlarged and the signals are shifted in the time domain, thus both the PAPR and the phase noises are reduced, and the RCFO can be mitigated. Furthermore, we derive the analytical signal-to-interference-plus-noise ratio (SINR) expressions for bit error rate (BER) performance analysis. Numerical simulations verify the effectiveness of our theoretical analysis of SINR. Additionally, we demonstrate that the presented robust HRCI and DRCI coded OFDM systems can suppress the PAPR satisfactorily and better BER performances can be achieved by the recursive CI-aided spread OFDM systems with phase noise rejection and RCFO compensation when compared with counterpart systems.**

***Index Terms*—Recursive carrier interferometry spreading code; Hadamard recursion; Diagonal recursion; Peak to average power ratio; Phase noise rejection; Residual carrier frequency offset compensation.**

I. Introduction

In recent years, orthogonal frequency division multiplexing (OFDM) transmission technique has been widely used to meet the increasing demands for high data rate access to multi-media services. However, high speed OFDM transmissions will lead to higher peak to average power ratio (PAPR) of the transmitted OFDM signals and narrower sub-carrier phase intervals in a specified band. Additionally, OFDM systems will be more sensitive to carrier frequency drifting, thus degrading the performance of the wireless system.

The spread orthogonal frequency division multiplexing (SOFDM) scheme has been proposed to enhance the performances of OFDM system over multipath fading channels by exploiting the diversity gain [1], with additional benefit of suppressing PAPR of the OFDM signals. In [2], a discrete fourier transform (DFT) scheme is presented for SOFDM systems, and the PAPR in DFT-SOFDM system can be suppressed for single carrier frequency division multiplexing access (SC-FDMA) systems. Then, the PAPR is further lowered by [3] and [4], which respectively propose to apply zero-tail DFT-SOFDM and unique word DFT-SOFDM to replace cyclic prefix for better tail characteristics to achieve better bit error rate (BER) performances in rich scattering environment. However, in DFT-SOFDM systems, some bands are used for transmitting the specified sequences to attain low PAPR [5], which results in bandwidth wastage and leads to a lower spectral efficiency. The carrier interferometry (CI) codes can be used as spreading codes in SOFDM systems to suppress PAPR with high spectral efficiency [6]–[8]. On one hand, the CI codes would not require to use additional sub-bands to transmit the specified sequences, and could spread OFDM symbols over all N subcarriers to suppress PAPR, thus the spectral efficiency is attained without performance losses. On the other hand, compared with other spreading codes such as Hadamard-Walsh code [6], the CI spreading code can be designed in a more flexible way according to the number of subcarriers of any integer value. Moreover, non-contiguous CI codes can be applied in dynamic spectrum access cognitive radio network [6] to eliminate the loss of orthogonality among spreading codes caused by deactivating sub-carriers. Thus with higher spectral utilization and spectral efficiency, the CI coded systems can achieve lower PAPR and better BER performances over frequency-selective fading channel [7] by suppressing the narrowband interferences [8].

However, high speed spread OFDM systems may suffer from smaller phase intervals between signals over different subcarriers in the specified band and become more sensitive to carrier frequency drifting. In other words, when the sub-carrier number increases, the phase intervals would become smaller, which leads to the performance degradation in the presence of phase noise and residual carrier frequency offset (RCFO). Besides, as indicated by [15], since the impact of the phase noise can become even more profound when the systems operate at higher carrier frequencies, such as $E-band/70-80GHz$, it is increasingly important to develop efficient detection algorithms for compensating the effect of the carrier frequency offset (CFO) and the phase noise in high data rate OFDM systems with large bandwidth and densely spaced sub-carriers.

The phase noise is a random process caused by the fluctuation of the receiver and transmitter oscillators. In OFDM systems, phase noises will induce the loss of orthogonality between subcarriers [9]. Pollet $et\ al.$ analytically evaluated the influence of CFO and carrier phase noise on the BER performance degradation for OFDM systems [9]. Then, Wu $et\ al.$ presented a general phase-noise suppression scheme [10] and derived a closed-form expression for the signal-to-noise-plus-interference ratio (SINR) for exact performance analysis. Furthermore, in order to compensate the phase noises at OFDM receivers, Mathecken $et\ al.$ proposed phase noise estimation schemes that utilize the geometry associated with the spectral components of the complex exponential of phase noise [11], and [11] presented a new phase noise spectral model to evaluate the phase noise more exactly. Joint estimations of channel response, frequency offset, phase noise are also proposed for better estimation in realistic OFDM systems [12]–[15].

In addition, RCFO, which is caused by estimation errors of existing frequency offset recovery methods, will generate phase drift in each subcarrier and destroy the subcarrier orthogonality [16]. [17] analyzed the effect of RCFO on performance degradations. Then, Sliskovic proposed a pilot-aided sampling and carrier frequency offset estimator which derives the frequency estimates by comparing the phases of the pilots at the receiver side [18]. In addition, tracking possible RCFO and SFO variations during the data section of the frame is also helpful to improve the system performance and [19] proposed a new decision-directed synchronization scheme for carrier frequency offset estimations for OFDM systems.

Different from existing phase noise rejection schemes and RCFO compensation schemes for radio frequency (RF) systems, in this paper, we present recursive spreading CI code to simultaneously suppress PAPR and combat the phase noise as well as the RCFO for high speed OFDM systems over RF channels, thus both the reliability and the robustness of the system can be improved. In our previous work [20], we investigated the phase noise issue for optical OFDM systems. In this paper, we propose a generalized algorithm to construct the recursive CI codes to simultaneously suppress PAPR, reject the phase noises and compensate the carrier frequency offset for high speed RF OFDM systems.

Specifically, we propose a recursive spread code generation algorithm and two new recursive CI codes, which are called long Hadamard recursive CI (HRCI) and Diagonal recursive CI (DRCI) codes. Hadamard recursion is a general matrix extension process which realizes the extension of Hadamard matrices [21], and the resultant HRCI codes have multiple elements and their phases are different, which are different from conventional Hadamard matrices whose elements are 1 or -1. In addition, we apply diagonal recursion, which is a matrix extension process of calculating the Kronecker product of 2 order identity matrix and CI code matrix, and present DRCI codes. Then, we prove that both HRCI codes and DRCI codes inherit the benefits of conventional CI code, including the invertibility and orthogonality properties of the generation matrices during the recursion process.

Furthermore, we analytically derive the SINR expressions based on the phase noise model in [10] and the RCFO model in [16] to evaluate the performances of systems using our presented HRCI codes and DRCI codes. More specifically, we firstly derive the expression of demodulated signal based on these models. By separating the information-bearing signal and the interferences from the received data, we conduct an analytical analysis on the formulations of received signal. Then, the SINR expression can be obtained by calculating the average power of information-bearing signals and the interferences induced to the received data.

More explicitly, except for the analysis of the phase noise and RCFO issue for high speed OFDM systems, the main contributions of this paper include: (1) based on the recursion principle, we present recursive spreading HRCI codes and DRCI codes in complex domain to enlarge the phase intervals between transmitted signals; (2) we prove that the invertibility properties of generation matrices constructed with Hadamard recursion and diagonal recursion are held during recursions; and (3) we derive SINR expressions for the theoretical performance analysis.

The rest of the paper is organized as follows. We first introduce the SOFDM system model and the issues of phase noise and RCFO. Subsequently, in Section III we present the recursive spreading code design, and propose two novel types of Hadamard recursion and diagonal recursion based spreading CI codes. Besides, we provide the theoretical analysis of the characteristic of Hadamard recursion and diagonal recursion. In Section IV, we apply the proposed HRCI and DRCI codes to SOFDM systems and decompose the demodulated signal into the information-bearing signals and interferences. Then, we derive the corresponding SINR for the received data. Section V provides simulation results to verify the effectiveness of theoretical analysis, and to analyze the reliability, PAPR and the robustness performances for the presented HRCI and DRCI coded SOFDM systems. Finally we conclude our findings in Section VI.

II. Spreading OFDM System Model

In this section, we firstly describe the spreading OFDM system and present the issues of phase noise and CFO in detail. Then, we provide the phase noise model, the CFO model, and the RCFO model as below.

A. System Model

Fig. 1 illustrates the block diagram of SOFDM system [6], [22]. At the transmitter side, after a serial-to-parallel (S/P) conversion, the data stream is mapped to data symbols. After spread by the codes expressed in terms of a $N \times N$ matrix $\mathbf{G}$, the data symbols are modulated by the N-point inverse fast Fourier transform (IFFT) module, wherein N denotes the subcarrier number. After performing cyclic prefix extensions and parallel-to-serial (P/S) conversions, the SOFDM transmitters output the information-bearing signals $x(t)$ for transmission over RF channels.

At the receiver side, after removing the cyclic prefix in the received signal $\mathbf{r}$, we apply the expectation conditional maximization (ECM) estimator proposed in [15] to jointly

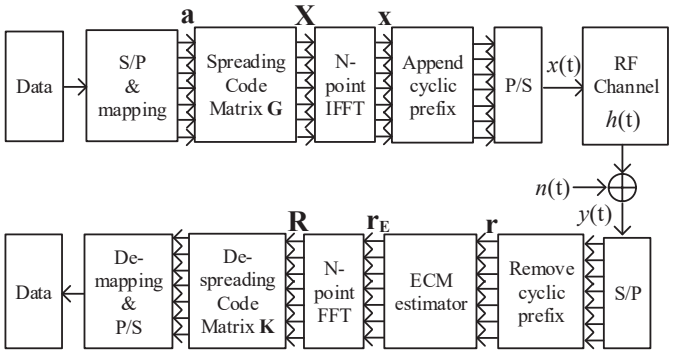

Fig. 1. SOFDM system.(S/P: serial to parallel; IFFT: inverse fast Fourier transform; P/S: parallel to serial; RF: radio frequency; ECM: expectation conditional maximization; FFT: discrete Fourier transform.)

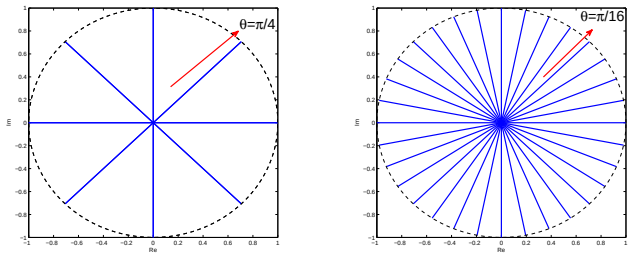

(a) M=8 (b) M=32

Fig. 2. Phase interval of CI code for different N.

estimate the channel state information, phase noise, and CFO in SOFDM systems. Thanks to the estimation of signal parameters, the equalizer is not required to be employed to mitigate the inter-symbol-interferences (ISI) as in [23]. Next, N-point fast Fourier transform (FFT) and the de-spreading code $N \times N$ matrix $\mathbf{K}$ are applied to the received signal to realize the de-spreading process. After de-mapping and P/S conversion, the transmitted data can be recovered.

More specifically, according to the definition of CI code given by [8]

$$\{\zeta_0^k, \zeta_1^k, \ldots, \zeta_{M-1}^k\} = \{e^{j\frac{2\pi}{M}\cdot k\cdot 0}, e^{j\frac{2\pi}{M}\cdot k\cdot 1}, \ldots, e^{j\frac{2\pi}{M}\cdot k\cdot (M-1)}\}, \quad (1)$$

where k indicates the k^{th} symbol's spreading sequence characterized by $\{\zeta_0^k, \zeta_1^k, \ldots, \zeta_{M-1}^k\}$. We rewrite CI code in a matrix form and the $M \times M$ conventional spreading CI code matrix $\mathbf{G_{CI}}$ is defined as

$$\mathbf{G_{CI}}_{i,l} = exp(-j\frac{2\pi}{M} i * l),\ 0 \le i, l \le M-1, \quad (2)$$

where $j = \sqrt{-1}$, $\mathbf{G_{CI}}_{i,l}$ is the the element in i^{th} row and l^{th} column of matrix $\mathbf{G_{CI}}$ and conventional de-spreading CI code matrix $\mathbf{K_{CI}}$ is

$$\mathbf{K_{CI}}_{i,l} = exp(j\frac{2\pi}{M} i * l),\ 0 \le i, l \le M-1. \quad (3)$$

The relation between subcarrier number N and the dimension of $\mathbf{G_{CI}}$ and $\mathbf{K_{CI}}$ will be discussed in III-A.

B. Phase Noise and CFO Issues for SOFDM Systems

In high speed SOFDM systems, in order to support high data rate, the subcarrier number is required to be large, thus the length of spreading code becomes longer and the phase intervals of signals over different subcarriers become smaller. Thereby the SOFDM systems become more sensitive to phase noise and carrier frequency drifting. Take the code length of $M = 8$ and $M = 32$ as an example. As shown in Fig. 2, phase intervals are respectively $\pi/4$ and $\pi/16$ for the CI codes with length of $M = 8$ and $M = 32$, which proves that phase intervals among CI codes increase as the length of CI code decreases. More explicitly, the definition of phase intervals among $N \times N$ matrix $\mathbf{A}$ is

$$\varphi = \min\left(\left|\arctan\left(\frac{\Im(\mathbf{A}_{i,l})}{\Re(\mathbf{A}_{i,l})}\right) - \arctan\left(\frac{\Im(\mathbf{A}_{i,l+1})}{\Re(\mathbf{A}_{i,l+1})}\right)\right|\right). \quad (4)$$
$$0 \le i \le N-1, \quad 0 \le l \le N-2$$

Due to the smaller phase interval among CI codes, large scale CI code based SOFDM systems are more sensitive to phase noise than those without CI code. In addition, the CFO generates the phase drift in each subcarrier and destroys the subcarrier orthogonality, which causes a even worse situation when the phase intervals become smaller.

Next, we provide the phase noise model, CFO model and baseband signal model.

C. Phase Noise and CFO Model

Phase noise θ, which occurs at both transmitter and receiver oscillators, can be presented as a finite-power Wiener process which has independent Gaussian increments [24]–[27]. In this paper, the phase noise model developed by Demir [28], which provides more accurate description by using a nonlinear method, is used to characterize phase noise as

$$\theta_n = \theta_{n-1} + \zeta_n,\ n = 1, \ldots N, \quad (5)$$

where θ_n denotes the phase noise at the n^{th} instant, $\zeta_n \sim N(0, \sigma_\zeta^2)$ is the phase noise innovation, $\sigma_\zeta^2 = 2\pi\beta T/N$ is the variance of the innovation process, β denotes the phase noise linewidth, T is the symbol period in OFDM system, N is the subcarrier number, and $R = N/T$ denotes the transmission data rate.

On the other hand, normalized CFO $\epsilon = \Delta f T$ is modeled as a uniformly distributed random variable over the range $\epsilon \in (-0.5, 0.5)$ [12], [29]. The CFO vector $\mathbf{E}$ is defined as

$$E(n) = e^{(j2\pi n\epsilon/N)},\ n = 0, 1, \ldots, N-1, \quad (6)$$

where $E(n)$ is the n^{th} element of $\mathbf{E}$ and illustrates the frequency offset of the n^{th} subcarrier.

D. ECM Estimator and RCFO model

In this paper, ECM estimator proposed in [15] is applied to received signal, which realizes joint estimation of channel state, phase noise, and CFO in SOFDM systems. The ECM based estimation is carried out in two steps. In the expectation or E-step, an extended Kalman filter (EKF) based estimator is

utilized to accurately track the phase noise over the training OFDM symbol. During the maximization or M-step, the channel state and CFO parameters are estimated by minimizing the derived negative log likelihood function.

As illustrated in [15], with the aid of ECM estimator, more reliable communication is achieved with low computation complexity. However, the impact of channel state, phase noise and CFO cannot be completely eliminated. Moreover, the impacts of channel state, phase noise and CFO after ECM estimator are characterize by new channel spectral response $\mathbf{H}'$, new phase noise ϕ and RCFO respectively.

More explicitly, new phase noise ϕ is characterize as

$$\phi_n = \phi_{n-1} + \delta_n,\ n = 1, \dots N, \tag{7}$$

where ϕ_n denotes the phase noise at the n^{th} instant, $\delta_n \sim N(0, \sigma_\delta^2)$ is the phase noise innovation, and we have $\sigma_\delta^2 < \sigma_\zeta^2$ with the aid of ECM estimator.

Subsequently, as to the RCFO, considering that the uniform random CFO estimation and compensation are applied at receiver [15], [29], [30], we here regard the RCFO as a Gaussian random variable [30]

$$\nu \sim N(0, \sigma_\nu^2), \tag{8}$$

where ν is the Gaussian random variable that describes RCFO and σ_ν^2 is the variance of ν.

E. Baseband Signal Model

As illustrated in Fig. 1, IFFT operations are performed on signals $\{X(k)\}_{k=0}^{N-1}$ over N subcarriers in the frequency domain to produce the corresponding N modulated signals in the time domain. The baseband signal can be expressed as

$$x(n) = \frac{1}{\sqrt{N}} \sum_{k=0}^{N-1} X(k) e^{\frac{j2\pi nk}{N}}. \tag{9}$$

At receiver, after the cyclic prefix removal, the received signal $\mathbf{r}$ is

$$r(n) = e^{j\theta(n)}[x(n) * \mathcal{F}^{-1}(H(k))] + z(n), \tag{10}$$

where $*$ and $\mathcal{F}^{-1}(.)$ represent the circular convolution and IFFT operations, respectively, while $z(n)$ indicates the additive white Gaussian noise (AWGN) with zero mean and variance σ^2. $H(k)$ is the frequency domain channel response which is determined by a specific channel. After ECM estimation process and N-point FFT, with the aid of received signal expression in [10], take the RCFO signal model of [16], [17] into consideration, we have the expression of $\mathbf{R}$ as

$$R(k) = X(k)H'(k)\Upsilon_1(k) + \Upsilon_2(k) + Z(k), \tag{11}$$

where $\Upsilon_1(k)$ denotes fading and phase shift of the transmitted signal caused by phase noise and RCFO, $\Upsilon_2(k)$ is interference caused by phase noise and RCFO, $Z(k)$ is frequency domain AWGN after FFT process. Since FFT does not change the noise energy, $Z(k)$ is still a Gaussian random variable with zero mean and variance σ^2. The expression of $\Upsilon_1(k)$ is

$$\Upsilon_1(k) = I(0) e^{j2\pi N_B k \nu_k / N} f_N(\nu_k), \tag{12}$$

and $\Upsilon_2(k)$ is expressed as

$$\Upsilon_2(k) = ICI(k) e^{j2\pi N_B k \nu_k / N} f_N(\nu_k). \tag{13}$$

In equations (12) and (13), $e^{j2\pi N_B k\nu_k/N} f_N(\nu_k)$ denotes fading and phase shift cause by RCFO. More explicitly, let ν_k denote the RCFO of the k^{th} subcarrier and $N_B = N + N_g$ denote the length of the time domain transmitted signals, thus we have

$$f_N(x) = e^{j\pi x(N-1)/N} \frac{sin(\pi x)}{N sin(\pi x/N)}. \tag{14}$$

In addition, the items $e^{j\pi\nu_k[2N_Bk+(N-1)]/N}$ and $\frac{sin(\pi\nu_k)}{Nsin(\pi\nu_k/N)}$ in (12) and (14) represent the phase rotations and amplitude variations brought by the RCFO respectively. In equations (12), $I(0)$ represents the effects of common phase error (CPE) cause by phase noise. Moreover, $I(p)$ is defined as [10]

$$I(p) = \frac{1}{N} \sum_{n=0}^{N-1} e^{j[\frac{2\pi pn}{N} + \phi(n)]}, \tag{15}$$

In equations (13), $ICI(k) = \Sigma_{l=0, l\neq k}^{N-1} X(l)H'(l)I(l-k)$ is inter-carrier-interference (ICI) cause by phase noise.

At last, the expression of $\Upsilon_1(k)$ and $\Upsilon_2(k)$ can be further derived as

$$\Upsilon_1(k) = \frac{1}{N} \sum_{n=0}^{N-1} \frac{sin(\pi\nu_k)}{Nsin(\pi\nu_k/N)} e^{j\{\pi\nu_k[2N_Bk+(N-1)]/N + \phi(n)\}} \tag{16}$$

$$\Upsilon_2(k) = \frac{1}{N} \sum_{n=0}^{N-1} \sum_{l=0, l\neq k}^{N-1} X(l)H'(l) \frac{sin(\pi\nu_k)}{Nsin(\pi\nu_k/N)} \cdot e^{j\{\pi[2(l-k)n + 2N_Bk\nu_k + (N-1)\nu_k]/N + \phi(n)\}} \tag{17}$$

III. Recursive HRCI code and DRCI code Design

In order to combat the phase noises and the RCFO presented above, in this section, we firstly present the recursive spreading CI code design, then, we give the construction details of HRCI codes and DRCI codes. Moreover, we analyze the properties of the recursive code generation matrices to investigate whether the presented spreading codes can be applied in SOFDM systems.

A. Recursive Spreading CI Code Design

We here propose to construct long spreading code with short codes via recursions. Let M denote the dimension of spreading code matrix, which is determined according to the number of subcarriers denoted by N, namely we have

$$N = 2^k M,\ 0 \leq k, \tag{18}$$

where k is selected to satisfy that N can be divided by 2^k.

Algorithm 1 describes the procedure of generating recursion-based spreading codes, and the Kronecker product [31] extension matrix for extending the code matrices is determined by the recursion type.

More explicitly, in Hadamard recursion process, $i = 1$ and Kronecker product extension matrix is $\mathbf{W} = \frac{1}{\sqrt{2}} \begin{bmatrix} 1 & 1 \\ 1 & -1 \end{bmatrix}$ which can realize Hadamard recursion for generating HRCI code. When another type of the diagonal recursion is applied, $i = 0$

Algorithm 1 Recursive spread code generation

1: **Initialisation:** Obtain k in (18), CI code matrices $\mathbf{G_{CI}}$, $\mathbf{K_{CI}}$ and recursion type $\mathbf{TYPE} = 'Hadamard'$ *or* $'diagonal'$. Set $i = 1$ for $\mathbf{TYPE} = 'Hadamard'$, $i = 0$ for $\mathbf{TYPE} = 'diagonal'$, spreading matrix $\mathbf{G} = \mathbf{G_{CI}}$, de-spreading matrix $\mathbf{K} = \mathbf{K_{CI}}$, $n = 0$.
2: **repeat**
3: Kronecker product extension matrix $\mathbf{W} = \left(\frac{1}{\sqrt{2}}\begin{bmatrix}1 & 1\\ 1 & -1\end{bmatrix}\right)^i$
4: Recursion for spreading matrix $\mathbf{G} = \mathbf{W} \otimes \mathbf{G}$.
5: Recursion for de-spreading matrix $\mathbf{K} = \mathbf{W} \otimes \mathbf{K}$.
6: $n = n + 1$
7: **until** $n = k$.
8: **return** $\mathbf{G}$ for spreading matrix and $\mathbf{K}$ for de-spreading matrix

and Kronecker product extension matrix is denoted by $\mathbf{W} = \left[\begin{smallmatrix}1 & 0\\ 0 & 1\end{smallmatrix}\right]$ which is the same as Eq. (25) and utilizes the diagonal recursion to generate the DRCI codes.

It is worth pointing out that the presented DRCI code and HRCI code inherit the PAPR suppression characteristic from traditional CI codes [6] which utilizes the complex exponential elements of CI codes to counteract the PAPR issue caused by IFFT. Note that the CI code matrix is essentially a FFT matrix, employing a full rank CI code cancels the IFFT and therefore provides a signal with the same PAPR as a single carrier transmission. Similar technologies such as single carrier FDMA (SC-FDMA) and single carrier transmission with frequency domain equalization have been proposed and developed to reduce the PAPR of multi-carrier transmissions. In the proposed schemes in this manuscript, the DRCI code and HRCI code do not eliminate the PAPR entirely like a full rank CI code, but it does reduce the PAPR significantly through inheritance of the PAPR suppression characteristic of traditional CI code.

Moreover, the presented DRCI code and HRCI code maintain the relatively larger phase intervals of short CI codes. To be more explicit, in Algorithm 1, after carrying out the logical OR operation of the normalized matrix $\mathbf{W}=\frac{1}{\sqrt{2}}\left[\begin{smallmatrix}1 & 1\\ 1 & -1\end{smallmatrix}\right]$ and the identity matrix, i.e., $\mathbf{W}=\frac{1}{\sqrt{2}}\left[\begin{smallmatrix}1 & 1\\ 1 & -1\end{smallmatrix}\right] \bigvee \left[\begin{smallmatrix}1 & 0\\ 0 & 1\end{smallmatrix}\right]$ where $\bigvee$ represents the logical OR operation, the value of the elements in the resultant matrix are typically $\{-1, 0, 1\}$. That is to say, Algorithm 1 recursively generates HRCI codes and DRCI codes using the elements in the matrices $\mathbf{G_{CI}}$ and $\mathbf{K_{CI}}$, thus the phase intervals of resultant DRCI codes and HRCI codes are the same as those of short CI code matrices $\mathbf{G_{CI}}$ and $\mathbf{K_{CI}}$.

Thus, thanks to enlarged phase intervals, the presented DRCI code and HRCI code can combat the phase noises and the CFO, thus they have the capability of the phase noise rejection and the RCFO mitigation while effectively suppressing the PAPR.

Take $k = 2$ and $N = 4M$ as an example. The details of the corresponding spreading and de-spreading code design based on Algorithm 1 is given as below.

B. Hadamard Recursion and HRCI Code Design

It is well known that high order Hadamard matrix can be generated from a low order one by Hadamard recursion [21]. Assuming $\mathbf{H}$ is a Hadamard matrix of order n, Hadamard recursion is defined as

$$\mathbf{H_{2n}} = \begin{bmatrix}\mathbf{H} & \mathbf{H}\\ \mathbf{H} & -\mathbf{H}\end{bmatrix}, \tag{19}$$

where $\mathbf{H_{2n}}$ is a Hadamard matrix of order $2n$.

Using the CI code given by (2), we propose to generate the HRCI codes in the following way

$$\mathbf{G_{2M,H}} = \begin{bmatrix}\mathbf{G_{CI}} & \mathbf{G_{CI}}\\ \mathbf{G_{CI}} & -\mathbf{G_{CI}}\end{bmatrix}, \mathbf{G_{4M,H}} = \begin{bmatrix}\mathbf{G_{2M,H}} & \mathbf{G_{2M,H}}\\ \mathbf{G_{2M,H}} & -\mathbf{G_{2M,H}}\end{bmatrix}. \tag{20}$$

After the normalization, the HRCI spreading code matrix $\mathbf{G_H}$ is expressed as

$$\mathbf{G_H} = \frac{1}{\sqrt{N}}\mathbf{G_{4M,H}}. \tag{21}$$

Similarly, the de-spreading code matrix can be generated through

$$\mathbf{K_{2M,H}} = \begin{bmatrix}\mathbf{K_{CI}} & \mathbf{K_{CI}}\\ \mathbf{K_{CI}} & -\mathbf{K_{CI}}\end{bmatrix}, \mathbf{K_{4M,H}} = \begin{bmatrix}\mathbf{K_{2M,H}} & \mathbf{K_{2M,H}}\\ \mathbf{K_{2M,H}} & -\mathbf{K_{2M,H}}\end{bmatrix}, \tag{22}$$

and the HRCI de-spreading code matrix $\mathbf{K_H}$ is

$$\mathbf{K_H} = \frac{1}{\sqrt{N}}\mathbf{K_{4M,H}}. \tag{23}$$

C. Diagonal Recursion and DRCI Code Design

Similar to the Hadamard recursion, the diagonal recursion can also be applied to generate high order matrix from a low order one and hold the matrix invertibility property.

Assuming $\mathbf{D}$ is a square matrix of order n, the definition of diagonal recursion is

$$\mathbf{D_{2n}} = \begin{bmatrix}\mathbf{D} & \mathbf{0_n}\\ \mathbf{0_n} & \mathbf{D}\end{bmatrix}, \tag{24}$$

where $\mathbf{D_{2n}}$ is a high order matrix of order $2n$. More explicitly, the diagonal recursion process can be realized by calculating the Kronecker product [31] of a 2-order identity matrix and a low order matrix as

$$\mathbf{D_{2n}} = \begin{bmatrix}1 & 0\\ 0 & 1\end{bmatrix} \otimes \mathbf{D} = \begin{bmatrix}\mathbf{D} & \mathbf{0_n}\\ \mathbf{0_n} & \mathbf{D}\end{bmatrix}, \tag{25}$$

where $\otimes$ indicates Kronecker product.

Utilizing diagonal recursion in (24) and CI code in (2), the spreading code matrix can be generated through

$$\mathbf{G_{2M,D}} = \begin{bmatrix}\mathbf{G_{CI}} & \mathbf{0_M}\\ \mathbf{0_M} & \mathbf{G_{CI}}\end{bmatrix}, \mathbf{G_{4M,D}} = \begin{bmatrix}\mathbf{G_{2M,D}} & \mathbf{0_{2M}}\\ \mathbf{0_{2M}} & \mathbf{G_{2M,D}}\end{bmatrix}. \tag{26}$$

After the normalization, the DRCI spreading code matrix $\mathbf{G_D}$ is expressed as

$$\mathbf{G_D} = \frac{1}{\sqrt{M}}\mathbf{G_{4M,D}}. \tag{27}$$

Similarly, the de-spreading code matrix can be generated through

$$\mathbf{K_{2M,D}} = \begin{bmatrix}\mathbf{K_{CI}} & \mathbf{0_M}\\ \mathbf{0_M} & \mathbf{K_{CI}}\end{bmatrix}, \mathbf{K_{4M,D}} = \begin{bmatrix}\mathbf{K_{2M,D}} & \mathbf{0_{2M}}\\ \mathbf{0_{2M}} & \mathbf{K_{2M,D}}\end{bmatrix}, \tag{28}$$

and the DRCI de-spreading code matrix $\mathbf{K_D}$ is

$$\mathbf{K_D} = \frac{1}{\sqrt{M}}\mathbf{K_{4M,D}}. \tag{29}$$

D. Invertibility Property Analysis for Recursive Spreading CI Codes

Considering that the invertibility of the spreading code matrix is required in SOFDM system for de-spreading when recovering the received data, we will prove that the invertibility property is held during both Hadamard recursion and Diagonal recursion as follows.

Theorem 1. *Matrix invertibility property is held during the Hadamard recursion.*

Proof: Assuming $\mathbf{Z}$ is an n order nonsingular matrix, we have $\mathbf{Z^{-1}Z} = \mathbf{I_n}$ where $\mathbf{Z^{-1}}$ is the inverse matrix of $\mathbf{Z}$ and $\mathbf{I_n}$ is an n order identity matrix. The zero elements in $\mathbf{I_n}$ can be calculated by

$$(\mathbf{Z^{-1}Z})_{i,j,\ i\neq j} = \sum_{k=1,i\neq j}^{n} \mathbf{Z}^{-1}_{i,k}\mathbf{Z}_{k,j} = 0. \tag{30}$$

Utilizing (19), a high order matrix of $2n$ generated by Hadamard recursion from $\mathbf{Z}$ can be expressed as

$$\mathbf{Y}=\begin{bmatrix}\mathbf{Z} & \mathbf{Z}\\ \mathbf{Z} & -\mathbf{Z}\end{bmatrix}, \tag{31}$$

$$\mathbf{Y}_{i,j}=\begin{cases}\mathbf{Z}_{i,j}, & 1\le i\le n, 1\le j\le n\\ \mathbf{Z}_{i,j-n}, & 1\le i\le n, n+1\le j\le 2n\\ \mathbf{Z}_{i-n,j}, & n+1\le i\le 2n, 1\le j\le n\\ -\mathbf{Z}_{i-n,j-n}, & n+1\le i\le 2n, n+1\le j\le 2n\end{cases}. \tag{32}$$

Similarly, applying Hadamard recursion, $\mathbf{Z^{-1}}$ can be extended as

$$\mathbf{P}=\begin{bmatrix}\mathbf{Z^{-1}} & \mathbf{Z^{-1}}\\ \mathbf{Z^{-1}} & -\mathbf{Z^{-1}}\end{bmatrix}. \tag{33}$$

As for $1\le i\le n, 1\le j\le n$, utilizing (30) and (32), the result of $\mathbf{PY}$ is

$$\begin{aligned}(\mathbf{PY})_{i,j}&=\sum_{k=1}^{2n}\mathbf{P}_{i,k}\mathbf{Y}_{k,j}=\sum_{k=1}^{n}\mathbf{P}_{i,k}\mathbf{Y}_{k,j}+\sum_{k=n+1}^{2n}\mathbf{P}_{i,k}\mathbf{Y}_{k,j}\\ &=\sum_{k=1}^{n}\mathbf{Z}^{-1}_{i,k}\mathbf{Z}_{k,j}+\sum_{k=1}^{n}\mathbf{Z}^{-1}_{i,k}\mathbf{Z}_{k,j}\\ &\Rightarrow \mathbf{PY}=2\mathbf{I_n},\ 1\le i\le n, 1\le j\le n\end{aligned}. \tag{34}$$

Similarly, we have

$$(\mathbf{PY})_{i,j}=\begin{cases}\mathbf{0_n}, & 1\le i\le n, n+1\le j\le 2n\\ \mathbf{0_n}, & n+1\le i\le 2n, 1\le j\le n\\ 2\mathbf{I_n}, & n+1\le i\le 2n, n+1\le j\le 2n\end{cases}, \tag{35}$$

where $\mathbf{0_n}$ is an order n zero matrix. Thus, we have

$$\mathbf{PY} = 2\mathbf{I_{2n}}, \tag{36}$$

where $\mathbf{I_{2n}}$ is a $2n$ order identity matrix.

Taking the normalization factor $1/\sqrt{2}$ in Algorithm 1 into consideration, we can come to a conclusion from (36) that $\mathbf{P}$ is the inverse matrix of $\mathbf{Y}$ and matrix inverse property is held during Hadamard recursion. The proof is completed. ■

Theorem 2. *Matrix inverse property is held during diagonal recursion.*

Proof: Assuming $\mathbf{D}$ is a n order nonsingular matrix, we have $\mathbf{D^{-1}D} = \mathbf{I_n}$ where $\mathbf{D^{-1}}$ is the inverse matrix of $\mathbf{D}$ and $\mathbf{I_n}$ is an order n identity matrix. The zero elements in $\mathbf{I_n}$ can be calculated by

$$(\mathbf{D^{T}D})_{i,j,\ i\neq j} = \sum_{k=1,i\neq j}^{n} \mathbf{D}_{k,i}\mathbf{D}_{k,j} = 0. \tag{37}$$

According to (24), the element of $\mathbf{D_{2n}}$ can be expressed as

$$(\mathbf{D_{2n}})_{i,j}=\begin{cases}\mathbf{D}_{i,j}, & 1\le i\le n, 1\le j\le n\\ 0, & 1\le i\le n, n+1\le j\le 2n\\ 0, & n+1\le i\le 2n, 1\le j\le n\\ \mathbf{D}_{i-n,j-n}, & n+1\le i\le 2n, n+1\le j\le 2n\end{cases}. \tag{38}$$

Applying the diagonal recursion, a high order matrix generated from $\mathbf{D^{-1}}$ can be extended as

$$\mathbf{Q}=\begin{bmatrix}\mathbf{D^{-1}} & \mathbf{0_n}\\ \mathbf{0_n} & \mathbf{D^{-1}}\end{bmatrix}. \tag{39}$$

Similar to (34) and (35), we have

$$(\mathbf{QD_{2n}})_{i,j}=\begin{cases}\mathbf{I_n}, & 1\le i\le n, n+1\le j\le 2n\\ \mathbf{0_n}, & 1\le i\le n, n+1\le j\le 2n\\ \mathbf{0_n}, & n+1\le i\le 2n, 1\le j\le n\\ \mathbf{I_n}, & n+1\le i\le 2n, n+1\le j\le 2n\end{cases}. \tag{40}$$

Thus, we have the similar result as (36)

$$\mathbf{QD_{2n}} = \mathbf{I_{2n}}, \tag{41}$$

which indicates $\mathbf{Q}$ is the inverse matrix of $\mathbf{D_{2n}}$ and the matrix invertibility property is held during diagonal recursions. The proof is completed. ■

E. Computational Complexity Analysis for Recursive Spreading CI Codes

In this subsection, the computational complexity of recursive spreading CI codes is compared with that of conventional CI code. Moreover, the comparison of the computational complexity of SOFDM and OFDM is provided.

Firstly, as illustrated in Section II-B conventional CI codes of length N are generated through equation (2) and (3) whose computational complexity are $O(N^2)$.

The recursive spread code generation process illustrated in Algorithm 1 is expressed as

$$\begin{aligned}\mathbf{G} &= \underbrace{\mathbf{W}\otimes\mathbf{W}\otimes\ldots\otimes\mathbf{W}}_{k}\otimes\mathbf{G_{CI}}\\ &= \mathbf{W^{(k)}}\otimes\mathbf{G_{CI}}\end{aligned}, \tag{42}$$

where $\mathbf{W^{(k)}} = \underbrace{\mathbf{W}\otimes\mathbf{W}\otimes\ldots\otimes\mathbf{W}}_{k}$. More explicitly, the computational complexity of calculating Kronecker product is determined by the size of the product matrix which can be expressed as

$$\mathbf{C}=\mathbf{A}\otimes\mathbf{B}, Size(\mathbf{C})=(N,M)\Longrightarrow Com=MN. \tag{43}$$

Therefore, computational complexity of recursive spreading CI codes generation is

$$Com_{RCI} = \underbrace{4^2+8^2+\ldots(2^k)^2}_{Com\ of\ \mathbf{W^{(k)}}} + \underbrace{N^2+M^2}_{Com\ of\ \mathbf{G_{CI}}} = O(N^2), \tag{44}$$

which is in the same order as conventional long CI codes.

Secondly, the computational complexities caused by spreading and de-spreading processes in SOFDM system in Fig. 1 are determined by the complexity of matrix multiplication of $N \times N$ matrix and $N \times 1$ vector which is $O(N^2)$.

Finally, the computational complexity of the proposed recursive spreading CI codes in SOFDM system is $O(N^2)$, which is much lower than the computational complexity of the data detection algorithms $O(N^3)$ in [15], [32].

IV. Theoretical Performance Analysis

In this section, we firstly describe the spread and de-spread signal based on the system model given in Section II-A and the recursive spreading code design presented in Section III, then, we analyze the SINR of SOFDM systems.

A. Spread and De-spread Signal

As illustrated in Fig. 1, at the transmitter, the spreading code matrix $\mathbf{G}$ is applied to data $\mathbf{a}$, while at the receiver, the de-spreading code matrix $\mathbf{K}$ is applied to the received signal to obtain demodulated signal $\mathbf{b}$. Thus we have

$$\begin{aligned} X(k) &= \frac{1}{\sqrt{N}} \sum_{i=0}^{N-1} a_i \mathbf{G}_{i,k}, \\ b(q) &= \frac{1}{\sqrt{N}} \sum_{k=0}^{N-1} R(k) \mathbf{K}_{k,q}. \end{aligned} \tag{45}$$

Substituting (11) into (45), the demodulated signal is obtained as

$$\begin{aligned} b(q) &= \tfrac{1}{N} \textstyle\sum_{k=0}^{N-1} \sum_{i=0}^{N-1} a_i \mathbf{G}_{i,k} \mathbf{K}_{k,q} H'(k) \Upsilon_1(k) + \tfrac{1}{\sqrt{N}} \sum_{k=0}^{N-1} Z(k) \mathbf{K}_{k,q} \\ &+ \frac{1}{N} \sum_{k=0}^{N-1} \sum_{i=0}^{N-1} \sum_{l=0,l\neq k}^{N-1} a_i \mathbf{G}_{i,l} \mathbf{K}_{k,q} H'(l) I(l-k) e^{j2\pi N_B k \nu_k / N} f_N(\nu_k). \end{aligned} \tag{46}$$

B. SINR Analysis

It can be seen from (46) that the demodulated signal $b(q)$ is constituted by the information-bearing signal, which contains a_q, and the interferences. Thus the first term of (46) becomes

$$\begin{aligned} &\frac{1}{N} \sum_{k=0}^{N-1} \sum_{i=0}^{N-1} a_i \mathbf{G}_{i,k} \mathbf{K}_{k,q} H'(k) \Upsilon_1(k) \\ &= \frac{1}{N} \sum_{k=0}^{N-1} \sum_{i=0,i\neq q}^{N-1} a_i \mathbf{G}_{i,k} \mathbf{K}_{k,q} H'(k) \Upsilon_1(k), \\ &+ \frac{1}{N} \sum_{k=0}^{N-1} a_q \mathbf{G}_{q,k} \mathbf{K}_{k,q} H'(k) \Upsilon_1(k) \end{aligned} \tag{47}$$

and the third term is

$$\begin{aligned} &\frac{1}{N} \sum_{k=0}^{N-1} \sum_{i=0}^{N-1} \sum_{l=0,l\neq k}^{N-1} a_i \mathbf{G}_{i,l} \mathbf{K}_{k,q} H'(l) I(l-k) e^{j2\pi N_B k \nu_k / N} f_N(\nu_k) \\ =& \frac{1}{N} \sum_{k=0}^{N-1} \sum_{i=0,i\neq q}^{N-1} \sum_{l=0,l\neq k}^{N-1} a_i \mathbf{G}_{i,l} \mathbf{K}_{k,q} H'(l) I(l-k) e^{j2\pi N_B k \nu_k / N} f_N(\nu_k). \\ &+ \frac{1}{N} \sum_{k=0}^{N-1} \sum_{l=0,l\neq k}^{N-1} a_q \mathbf{G}_{q,l} \mathbf{K}_{k,q} H'(l) I(l-k) e^{j2\pi N_B k \nu_k / N} f_N(\nu_k) \end{aligned} \tag{48}$$

Therefore, $\mathbf{b}$ can be expressed as

$$\begin{aligned} b(q) &= \frac{a_q}{N} \sum_{k=0}^{N-1} [\mathbf{G}_{q,k} \mathbf{K}_{k,q} H'(k) I(0) \\ &+ \sum_{l=0,l\neq k}^{N-1} \mathbf{G}_{q,l} \mathbf{K}_{k,q} H'(l) I(l-k)] e^{j2\pi N_B k \nu_k / N} f_N(\nu_k) \\ &+ \frac{1}{N} \sum_{k=0}^{N-1} \sum_{i=0,i\neq q}^{N-1} [a_i \mathbf{G}_{i,k} \mathbf{K}_{k,q} H'(k) I(0) \\ &+ \sum_{l=0,l\neq k}^{N-1} a_i \mathbf{G}_{i,l} \mathbf{K}_{k,q} H'(l) I(l-k)] e^{j2\pi N_B k \nu_k / N} f_N(\nu_k) \\ &+ \frac{1}{\sqrt{N}} \sum_{k=0}^{N-1} Z(k) \mathbf{K}_{k,q} \\ &= b_d(q) + b_i(q) + Z_n(q) \end{aligned} \tag{49}$$

where the information-bearing signal are the terms that contain a_q

$$\begin{aligned} b_d(q) &= \frac{a_q}{N} \sum_{k=0}^{N-1} [\mathbf{G}_{q,k} \mathbf{K}_{k,q} H'(k) I(0) \\ &+ \sum_{l=0,l\neq k}^{N-1} \mathbf{G}_{q,l} \mathbf{K}_{k,q} H'(l) I(l-k)] e^{j2\pi N_B k \nu_k / N} f_N(\nu_k) \end{aligned} \tag{50}$$

The second term of (50) can be derived as

$$\begin{aligned} &\frac{a_q}{N} \sum_{k=0}^{N-1} \sum_{l=0,l\neq k}^{N-1} \mathbf{G}_{q,l} \mathbf{K}_{k,q} H'(l) I(l-k) e^{j2\pi N_B k \nu_k / N} f_N(\nu_k) \\ &= \frac{a_q}{N} \sum_{k=0}^{N-1} [\sum_{l=0}^{N-1} \mathbf{G}_{q,l} \mathbf{K}_{k,q} H'(l) I(l-k) \\ &\quad - \underbrace{\mathbf{G}_{q,k} \mathbf{K}_{k,q} H'(k) I(0)}_{l=k}] e^{j2\pi N_B k \nu_k / N} f_N(\nu_k) \end{aligned} \tag{51}$$

Obviously, the second term in (51) is the same as the first term of (50) and therefore the expression of information-bearing signal is simplified as

$$b_d(q) = \tfrac{a_q}{N} \textstyle\sum_{k=0}^{N-1} \sum_{l=0}^{N-1} \mathbf{G}_{q,l} \mathbf{K}_{k,q} H'(l) I(l-k) e^{j2\pi N_B k \nu_k / N} f_N(\nu_k). \tag{52}$$

Similarly, the interference in (49) is represented as

$$\begin{aligned} b_i(q) &= \frac{1}{N} \sum_{k=0}^{N-1} \sum_{i=0,i\neq q}^{N-1} [a_i \mathbf{G}_{i,k} \mathbf{K}_{k,q} H'(k) I(0) \\ &+ \sum_{l=0,l\neq k}^{N-1} a_i \mathbf{G}_{i,l} \mathbf{K}_{k,q} H'(l) I(l-k)] e^{j2\pi N_B k \nu_k / N} f_N(\nu_k) \end{aligned} \tag{53}$$

and the corresponding simplified form is expressed as

$$\begin{aligned} b_i(q) &= \frac{1}{N} \sum_{k=0}^{N-1} \sum_{i=0,i\neq q}^{N-1} \sum_{l=0}^{N-1} a_i \mathbf{G}_{i,l} \mathbf{K}_{k,q} H'(l) \\ &\cdot I(l-k) e^{j2\pi N_B k \nu_k / N} f_N(\nu_k) \end{aligned} \tag{54}$$

Since the de-spreading matrices are normalized as illustrated in (23) and (29), the de-spreading process does not change signal energy and $Z_n(q)$ has the same properties as $Z(k)$.

Therefore, the SINR expression of SOFDM system is ob-

tained as

$$\Gamma = \frac{E[|b_d(q)|^2]}{E[|b_i(q)|^2] + \sigma^2}. \quad (55)$$

where $E[|b_i(q)|^2]$ and $E[|b_d(q)|^2]$ respectively represent the sinal and interference energy, which are derived in detail in Appendix A. From the energy evaluation expressions given by Eq .(A6) and Eq .(A7), we can see that the system performances are dependent on the spreading codes employed, the phase noise variances and the statistic of RCFO.

V. Performance Analysis and Simulations

In this section, the performances of the proposed HRCI codes and DRCI codes aided SOFDM systems in the presence of phase noise and CFO are evaluated, and the performances of conventional CI code aided SOFDM systems are also provided as a reference. For performance comparison, we set the same parameters as in reference [15]. The main simulation parameters are summarized in Table I. More explicitly, the unknown normalized CFO is assumed to be uniformly distributed over range $\epsilon \in (-0.5, 0.5)$ for each simulation and the data symbols are drawn from normalized 64 quadrature amplitude modulation (QAM).

TABLE I
Simulation parameters.

Parameters	Value
Modulation order	64QAM
Channel fading	Rayleigh
Channel taps	L=4
Channel taps power	[-1.52,-6.75,-11.91,-17.08]dB
Phase noise variance	$\sigma_\zeta^2 = [10^{-3}, 10^{-4}] rad^2$
CFO	U(-0.5,0.5)
Sampling rate	20MHz

We firstly simulate the BER performances of SOFDM systems using different spreading codes over frequency selective Rayleigh fading channel under different phase noise variance and compare them with existing algorithms in the references [12], [15], [32], [33]. Then, we analyze the corresponding SINR performance. Subsequently, BER performance of different spreading codes aided SOFDM systems with different lengths of short CI codes are provided. Next, the comparison of the phase interval for CI code, HRCI and DRCI codes with different code length is provided. Finally, we analyze the PAPR performances of the SOFDM systems using the presented recursion based spreading codes and compare them with the counterpart system given in [34].

In the simulations, as mentioned above, the phase noise, CFO model and ECM estimator are employed. Besides, we here assume RCFO is a Gaussian random process as given in (8).

A. Performances of SOFDM Systems at Different Phase Noise Variance

1) BER Comparison With Existing Work at Different Phase Noise: Firstly, we simulate the BER performances of SOFDM systems using different spreading codes over Rayleigh channel under different phase noise variance and compare them with existing algorithms. The following system setups are considered for comparison:

(i) The proposed HRCI code and DRCI code with ECM estimator in [15] (labelled as "HRCI" and "DRCI").
(ii) The estimation and data detection algorithm in [15] (labelled as " [15]").
(iii) The estimation and data detection algorithm in [12] and [32], respectively (labelled as " [12] & [32]").
(iv) The differential chaotic shift keying (DCSK) design with CI code [33] (labelled as " [33]").
(v) The conventional CI code(labelled as "CI").
(vi) As a lower-bound on the BER performance, a system assuming perfect channel, phase noise, and CFO estimation (labelled as "Perfect").

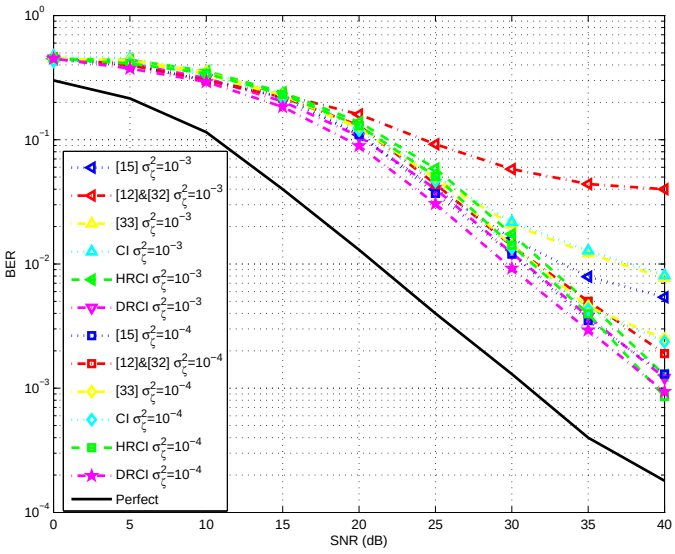

Fig. 3. Simulated BER performances of existing algorithm and SOFDM systems using CI, HRCI and DRCI codes over frequency selective Rayleigh fading channels with phase noises of different variances. The length of low order CI codes is $M = 16$.

Fig. 3 depicts the BER performance listed above. The following observations can be made from Fig. 3:

1) Compared to existing algorithms in [15], in the presence of very strong phase noise ($\sigma_\zeta^2 = 10^{-3} rad^2$), the BER performance of the proposed HRCI and DRCI codes are closer to the ideal case of perfect channel impulse response, phase noise, and CFO estimation (a performance gap of 6 dB at SNR = 40 dB), which indicates that the proposed HRCI and DRCI codes perform better than the data detection algorithm in [15]. On the other hand, the proposed HRCI and DRCI codes provide similar performance to the data detection algorithm in [15] in the presence of weak phase noise ($\sigma_\zeta^2 = 10^{-4} rad^2$).
2) It can be clearly observed that the proposed HRCI and DRCI codes outperform the algorithms in [12] and [32]. This performance improvement can be attributed to the fact that Algorithm 1 maintains the phase interval of the short CI code matrix and provide same phase noise robustness as short CI code. Moreover, the ECM estimator proposed in [15] also provides better estimation with the aid of EKF.

3) The existing algorithms in [33], which proposed DCSK design with CI code, provides similar BER performance to conventional CI code. It is clear that the performance of the proposed HRCI and DRCI codes outperform the algorithm in [33] and conventional CI code. This result is anticipated since Algorithm 1 maintains the phase interval of the short CI code matrix and provide the same phase noise robustness as short CI code. More explicitly, as illustrated in Fig. 2, the phase interval of the short CI code is larger than long CI code.

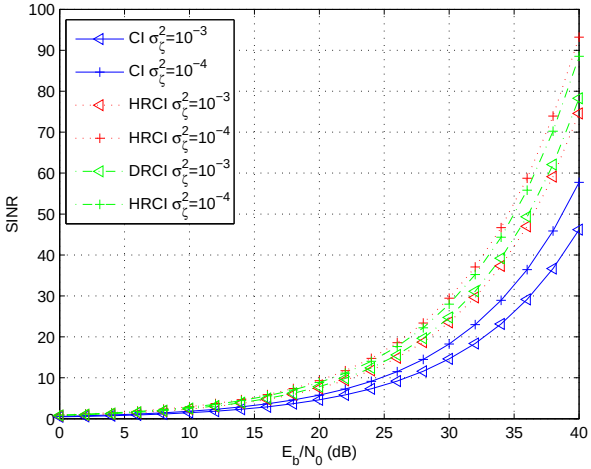

Fig. 4. SINR performances of SOFDM systems using CI, HRCI and DRCI codes over frequency selective Rayleigh fading channels with phase noises of different variances. The length of low order CI codes is $M = 16$.

2) SINR Performances: Next, the SINR performances of SOFDM system with different spreading codes are calculated by equation (55) and compared in Fig. 4. From equation (46), we can see that the expression of $b(q)$ changes with the specific combination of information signal $\mathbf{a}$. Hence we here simulate the SINR of the recursion-based CI coded SOFDM systems by calculating more than 10^7 transmitted frames, which provides an approximative mean value of SINR. The SINR performances in Fig. 4 show the same result as BER performances in Fig. 3, which proves better robustness can be achieved by using our HRCI and DRCI codes.

B. Performance at Different Size of Short CI Codes

Subsequently, we analyze the BER performances of SOFDM systems using HRCI and DRCI codes with different length of low order CI code $M = 4, 16, 64$, wherein the phase noise variance are set to $\sigma_\zeta^2 = [10^{-3}, 10^{-4}] rad^2$. As shown in Fig. 5, both HRCI and DRCI coded SOFDM systems achieve better performances when using shorter length low order CI code since the shorter length low order CI code has lager phase interval as illustrated in Section II-B and thus providing better noise tolerance. In addition, from Fig. 5, we can also observe that the HRCI coded system achieves similar BER performances to those of DRCI coded SOFDM systems with different length of low order CI code.

Next, Fig. 6 illustrates the comparison of phase interval for CI code, HRCI and DRCI codes with different code length N.

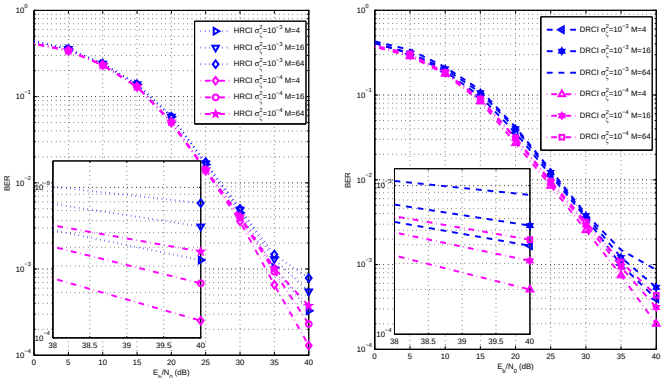

(a) HRCI (b) DRCI

Fig. 5. BER performances of SOFDM systems using the proposed HRCI and DRCI codes over frequency selective Rayleigh fading channels at different size of short CI codes.

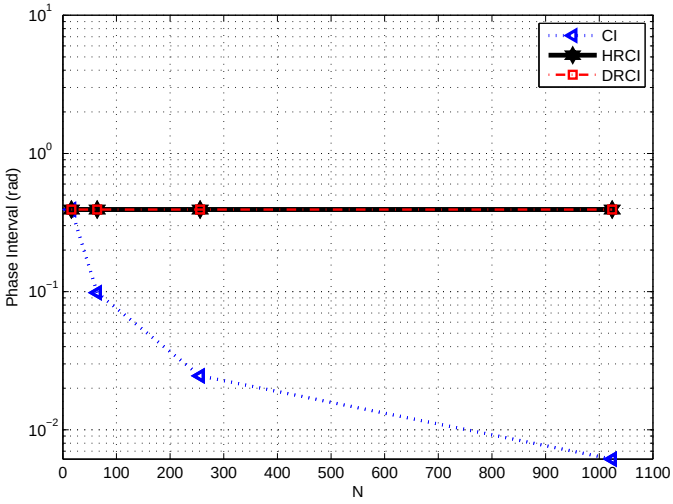

Fig. 6. Phase intervals of CI code, HRCI and DRCI codes with different N. $M = 16$.

It can be observed that the phase intervals of HRCI and DRCI codes remain the same as N increases, while those of CI codes decrease with the increasing N. The reason is that thanks to the generation process in Algorithm 1, the phase intervals of HRCI and DRCI codes are determined by the short CI code, thereby bringing the noise-resistant performance benefits to the SOFDM systems.

C. PAPR Performances and Comparisons

Fig. 7 illustrates the PAPR performances of SOFDM systems using 64QAM modulation and employing CI, HRCI and DRCI codes. It can be observed that with the aid of HRCI and DRCI codes, the PAPR performances have been improved about 2dB at possibility of 10^{-4} compared with the system without using spreading code in references [12], [15], [32]. Moreover, the SOFDM systems using recursion-based spreading codes achieve similar performances to the newly proposed PAPR reduction technique by using biased subcarriers in [34]. When compared with CI coded system and reference [33], HRCI and DRCI coded systems lost about 5dB of PAPR due to the Hadamard and diagonal recursion

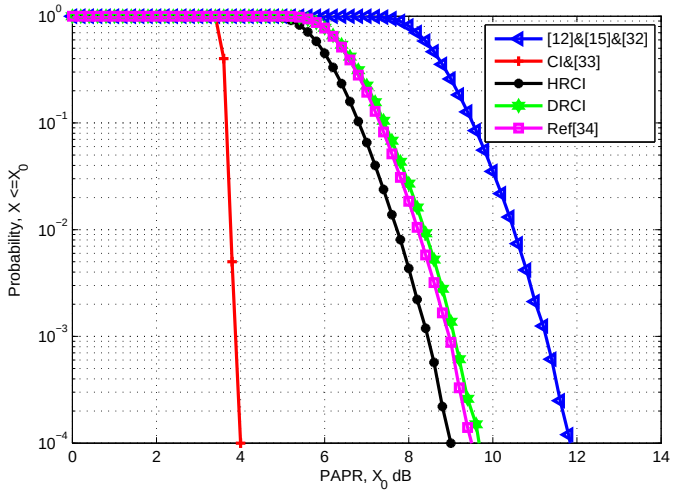

Fig. 7. The PAPR(CCDF) performances of SOFDM systems using CI, HRCI and DRCI codes. $M = 16$. (PAPR:peak-toaverage power ratio; CCDF:complementary cumulative distribution function.).

processes, which is acceptable considering the communication robustness enhancement in Fig. 3. More explicitly, reference [33] is an application of CI code which solves the PAPR issue of DCSK design and has the same PAPR performance as conventional CI code.

VI. Conclusion

In this paper, we present recursive HRCI and DRCI codes to combat the phase noises and RCFO existed in high speed SOFDM systems. With the aid of recursions, the high order HRCI and DRCI codes can be generated from low order CI codes, thus the phase intervals among the symbols are enlarged and more reliable communication performances than conventional high order one can be attained. We prove that the invertibility properties are held during the recursion procedure, which verifies the feasibility of applying the proposed HRCI codes and DRCI codes in both transmitters and receivers. Then, we analyze the SINR performances of HRCI and DRCI codes aided systems. Simulations are performed to investigate both the BER performances and the PAPR performances for our presented recursion-based transmission scheme design. Numerical results of BER as well as SINR verify that with the aid of HRCI and DRCI codes, the SOFDM systems are less sensitive to phase noises and RCFO, thereby achieving more reliable performances. Moreover, the simulation results also verify the effectiveness of our theoretical SINR analysis, and the PAPR performances are satisfactory compared with the counterpart schemes. Therefore, using the presented HRCI codes and DRCI codes, phase noises are reduced and RCFO is compensated, thus more reliable and more robust transmission capabilities can be achieved by SOFDM systems for the end users.

VII. Acknowledgements

This work was supported in part by the National Natural Science Foundation of China under Grant (No. 61602531 and No. 61572534), the National Science Foundation under (Grant No. 1323240), the Office of Naval Research (Contract N00024-14-C-4073). Huaiyin Lu wants to thank Ao Li's remarkable contribution in derivation of the expression of SINR. Finally, Huaiyin Lu wants to thank the invaluable support from Yi Liao.

Appendix A

As mentioned in Section IV, in order to evaluate the performances of the SOFDM systems employing the presented HRCI codes and DRCI codes, we here provide details of how to calculate $E[|b_i(q)|^2]$ and $E[|b_d(q)|^2]$ in the SINR evaluation expression given by Eq.(55).

Specifically, utilizing equation (54), $|b_i(q)|^2$ can be calculated by

$$|b_i(q)|^2 = \frac{1}{N^2}\sum_{k=0}^{N-1}\sum_{i=0,i\neq q}^{N-1}\sum_{l=0}^{N-1}\sum_{f=0}^{N-1}\sum_{p=0,p\neq q}^{N-1}\sum_{r=0}^{N-1} a_i a_p^* \mathbf{G}_{i,l}\mathbf{G}_{p,f}^*\mathbf{K}_{k,q}\mathbf{K}_{r,q}^* H'(l)H'^*(f)I(l-k) \cdot I^*(f-r)f_N(\nu_k)f_N^*(\nu_r)e^{j2\pi N_B(k\nu_k - r\nu_r)/N} \quad \text{(A1)}$$

Since the frequency domain channel response $H'(l)$ is independent from phase factor $I(l-k)$ and RCFO factor $e^{j2\pi N_B k\nu_k/N}f_N(\nu_k)$, after applying mean process $E(\cdot)$ to $|b_i(q)|^2$, we have

$$E[|b_i(q)|^2] = \frac{1}{N^3}\sum_{q=0}^{N-1}\sum_{k=0}^{N-1}\sum_{i=0,i\neq q}^{N-1}\sum_{l=0}^{N-1}\sum_{f=0}^{N-1}\sum_{p=0,p\neq q}^{N-1}\sum_{r=0}^{N-1} a_i a_p^* \mathbf{G}_{i,l}\mathbf{G}_{p,f}^*\mathbf{K}_{k,q}\mathbf{K}_{r,q}^* H'(l)H'^*(f)E[I(l-k)I^*(f-r)] \cdot f_N(\nu_k)f_N^*(\nu_r)e^{j2\pi N_B(k\nu_k - r\nu_r)/N} \quad \text{(A2)}$$

With the aid of equation (7), $E[e^{j\delta}]$ is calculated as

$$E[e^{j\delta}] = \int_{-\infty}^{+\infty} e^{j\delta}p(\delta)d\delta = \int_{-\infty}^{+\infty} e^{-j\delta t}p(\delta)d\delta|_{t=-1} = \frac{1}{\sqrt{2\pi}\sigma_\delta}\sqrt{2\pi\sigma_\delta^2}e^{-\frac{\sigma_\delta^2 t^2}{2}}|_{t=-1}| = e^{-\frac{\sigma_\delta^2}{2}} \quad \text{(A3)}$$

where $\delta \sim N(0,\sigma_\delta^2)$ and $p(\delta) = \frac{1}{\sqrt{2\pi}\sigma_\delta}e^{-\frac{\delta^2}{2\sigma_\delta^2}}$. Moreover, the expression of $E[I(s)I^*(w)]$ is

$$I(s)I^*(w) = \frac{1}{N^2}\sum_{n=0}^{N-1}\sum_{t=0}^{N-1} e^{j\frac{2\pi sn}{N}+j\phi_n}e^{-j\frac{2\pi wt}{N}-j\phi_t} = \frac{1}{N^2}\sum_{n=0}^{N-1}\sum_{t=0}^{N-1} e^{j\frac{2\pi}{N}(sn-wt)}e^{j(\phi_n-\phi_t)} \quad \text{(A4)}$$

$$E[I(s)I^*(w)] = \frac{1}{N^2}\sum_{n=0}^{N-1}\sum_{t=0}^{N-1} e^{j\frac{2\pi}{N}(sn-wt)}e^{-\frac{\sigma_\delta^2}{2}|n-t|}$$

The expression of $E[I(l-k)I^*(f-r)]$ is obtained by replacing s with $l-k$ and w with $f-r$ in (A4) as

$$E[I(l-k)I^*(f-r)] = \frac{1}{N^2}\sum_{n=0}^{N-1}\sum_{t=0}^{N-1} e^{j\frac{2\pi}{N}(ln+rt-kn-ft)}e^{-\frac{\sigma_\delta^2}{2}|n-t|}. \quad \text{(A5)}$$

Thus, the expression of $E[|b_i(q)|^2]$ is

$$E[|b_i(q)|^2] = \frac{1}{N^3}\sum_{q=0}^{N-1}\sum_{k=0}^{N-1}\sum_{i=0,i\neq q}^{N-1}\sum_{l=0}^{N-1}\sum_{f=0}^{N-1}\sum_{p=0,p\neq q}^{N-1}\sum_{r=0}^{N-1} a_i a_p^* \mathbf{G}_{i,l}\mathbf{G}_{p,f}^*\mathbf{K}_{k,q}\mathbf{K}_{r,q}^* H'(l)H'^*(f)e^{j\frac{2\pi}{N}(ln+rt-kn-ft)} \cdot e^{-\frac{\sigma_\delta^2}{2}|n-t|} f_N(\nu_k)f_N^*(\nu_r)e^{j2\pi N_B(k\nu_k-r\nu_r)/N} \quad \text{(A6)}$$

Similarly, the expression of $E[|b_d(q)|^2]$ is obtained as

$$E[|b_d(q)|^2] = \frac{1}{N^5}\sum_{q=0}^{N-1}\sum_{k=0}^{N-1}\sum_{l=0}^{N-1}\sum_{f=0}^{N-1}\sum_{r=0}^{N-1}\sum_{n=0}^{N-1}\sum_{t=0}^{N-1} |a_q|^2\mathbf{G}_{q,l}\mathbf{G}_{q,f}^*\mathbf{K}_{k,q}\mathbf{K}_{r,q}^* H'(l)H'^*(f)e^{j\frac{2\pi}{N}(ln+rt-kn-ft)} \cdot e^{-\frac{\sigma_\delta^2}{2}|n-t|} f_N(\nu_k)f_N^*(\nu_r)e^{j2\pi N_B(k\nu_k-r\nu_r)/N} \quad \text{(A7)}$$

REFERENCES

[1] G. Saulnier, Z. Ye, and M. Medley, "Performance of a spread spectrum OFDM system in a dispersive fading channel with interference," *1998 IEEE Military Communications Conference (MILCOM) Proceedings*, vol. 2, Oct. 1998.

[2] H. G. Myung, J. Lim, , and D. J. Goodman, "Peak-to Average Power Ratio of Single Carrier FDMA Signals with Pulse Shaping," *2006 IEEE 17th International Symposium on Personal, Indoor and Mobile Radio Communications(PIMRC)*, Sep. 2006.

[3] G. Berardinelli, F. Tavares, T. B. Sorensen, P. Mogensen, and K. Pajukoski, "Zero-tail DFT-spread-OFDM signals," *2013 IEEE Globecom Workshops (GC Wkshps)*.

[4] A. Sahin *et al.*, "An Improved Unique Word DFT-Spread-OFDM Scheme for 5G Systems," *2015 IEEE Globecom Workshops (GC Wkshps)*, Dec. 2015.

[5] G. Berardinelli, K. I. Pedersen, T. B. Sorensen, and P. Mogensen, "Generalized DFT-Spread-OFDM as 5G Waveform," *IEEE Commun. Mag.*, vol. 54, pp. 99–105, Nov. 2016.

[6] X. Li, V. Chakravarthy, B. Wang, and Z. Wu, "Spreading code design of adaptive non-contiguous SOFDM for dynamic spectrum access," *IEEE J. Sel. Topics Signal Process.*, vol. 5, pp. 190–196, Feb. 2011.

[7] D. Wiegandt, Z. Wu, and C. Nassar, "High capacity, high performance, low PAPR OFDM via carrier interferometry," *IEEE Trans. Commun.*, vol. 51, pp. 1123–1134, July. 2003.

[8] Z. Wu and C. Nassar, "Narrowband Interference Rejection in OFDM via Carrier Interferometry Spreading Codes," *IEEE Trans. Wireless Commun.*, vol. 4, pp. 1491–1505, July. 2005.

[9] T. Pollet, M. van Bladel, and M. Moeneclaey, "BER sensitivity of OFDM systems to carrier frequency offset and Wiener phase noise," *IEEE Trans. Commun.*, vol. 43, pp. 191–193, Feb. 1995.

[10] S. Wu and Y. Bar-Ness, "OFDM Systems in the Presence of Phase Noise: Consequences and Solutions," *IEEE Trans. Commun.*, vol. 52, pp. 1988–1996, Nov. 2004.

[11] P. Mathecken, T. Riihonen, S. Werner, and R. Wichman, "Phase noise estimation in OFDM: Utilizing its associated spectral geometry," *IEEE Trans. Signal Process.*, vol. 64, pp. 1999–2012, Apr. 2016.

[12] D. D. Lin and R. Pacheco and T. J. Lim and D. Hatzinakos, "Joint estimation of channel response, frequency offset, phase noise in OFDM," *IEEE Trans. Signal Process.*, vol. 54, pp. 3542–3554, Sep. 2006.

[13] D. D. Lin and T. J. Lim, "The variational inference approach to joint data detection and phase noise estimation in OFDM," *IEEE Trans. Signal Process.*, vol. 55, pp. 1862–1874, May. 2007.

[14] Y. Chi and A. Gomaa and N. Al-Dhahir and A. R. Calderbank, "Training signal design and tradeoffs for spectrally-effcient multi-user MIMO OFDM systems," *IEEE Trans. Wireless Commun.*, vol. 10, pp. 2234–2245, Jul. 2011.

[15] O. H. Salim and A. A. Nasir and H. Mehrpouyan and W. Xiang and S. Durrani and R. A. Kennedy, "Channel, phase noise, and frequency offset in OFDM systems: Joint estimation, data detection, and hybrid Cramér-Rao lower bound," *IEEE Trans. Commun.*, vol. 62, pp. 3311–3325, Sep. 2014.

[16] M. Morelli, G. Imbarlina, and M. Moretti, "Estimation of Residual Carrier and Sampling Frequency Offsets in OFDM-SDMA Uplink Transmissions," *IEEE Trans. Wireless Commun.*, vol. 9, pp. 734–744, Feb. 2010.

[17] C. Oberli, "ML-based Tracking Algorithms for MIMO-OFDM," *IEEE Trans. Wireless Commun.*, vol. 6, pp. 2630–2639, Feb. 2007.

[18] M. Sliskovic, "Carrier and sampling frequency offset estimation and correction in multicarrier systems," *in Proc. GLOBECOM 2001*, vol. 1, pp. 285–289, Feb. 2001.

[19] K. Shi, E. Serpedin, and P. Ciblat, "Decision-directed fine synchronization in OFDM systems," *IEEE Trans. Commun.*, vol. 53, pp. 408–412, Mar. 2005.

[20] H. Lu, L. Zhang, F. Fang, and Z. Wu, "Phase Noise Resistant Rotation Iteration Based Carrier Interferometry Code Design for High Speed Optical OFDM Systems," *IEEE Commun. Lett.*, vol. 22, pp. 522–525, Mar. 2018.

[21] J. Sylvester, "Thoughts on inverse orthogonal matrices, simultaneous sign successions, and tessellated pavements in two or more colours, with applications to Newton's rule, ornamental tile-work, and the theory of numbers," *Philos. Mag.*, vol. 34, no. 232, pp. 461–475, 1867.

[22] R. Rajbanshi, Q. Chen, A.Wyglinski, G. Minden, and J. Evans, "Quantitative comparison of agile modulation technique for cognitive radio tranceivers," *2007 4th IEEE Consumer Communications and Networking Conference (CCNC)*, pp. 1144–1148, Jan. 2007.

[23] A. Shalom and I. Tselniker and M. Nazarathy, "Improving the Phase Noise Tolerance of Subbanded DFT-Spread OFDM by Nonredundant Interleaving," *J. Lightw. Technol.*, vol. 32, pp. 4119–4132, Nov. 2014.

[24] M. S. El-Tanany, Y.Wu, and L. Hazy, "Analytical modeling and simulation of phase noise interference in OFDM-based digital television terrestrial broadcasting systems," *IEEE Trans. Broadcast.*, vol. 47, pp. 20–31, Mar. 2001.

[25] A. G. Armada and M. Calvo, "Phase noise and sub-carrier spacing effects on the performance of an OFDM communication system," *IEEE Commun. Lett.*, vol. 2, pp. 11–13, Jan. 1998.

[26] A. G. Armada, "Understanding the effects of phase noise in orthogonal frequency division multiplexing (OFDM)," *IEEE Trans. Broadcast.*, vol. 47, pp. 153–159, June. 2001.

[27] G. J. Foschini and G. Vannucci, "Characterizing filtered light waves corrupted by phase noise," *IEEE Trans. Inform. Theory*, vol. 34, pp. 1437–1448, Nov. 1988.

[28] A. Demir, A. Mehrotra, and J. Roychowdhury, "Phase noise in oscillators: A unifying theory and numerical methods for characterization," *IEEE Trans. Circuits Syst.*, vol. 47, pp. 655–674, May. 2000.

[29] M. Morelli and U. Mengali, "Carrier-frequency estimation for transmission over selective channels," *IEEE Trans. Commun.*, vol. 48, pp. 1580–1589, Sep. 2000.

[30] P. C. Weeraddana, N. Rajatheva, and H. Minn, "Probability of error analysis of BPSK OFDM systems with random residual frequency offset," *IEEE Trans. Commun.*, vol. 57, pp. 106–116, Sep. 2009.

[31] R. Bellman, *Introduction To Matrix Analysis*, ch. 20. New York: McGraw-Hill, 1960.

[32] P. Rabiei and W. Namgoong and N. Al-Dhahir, "A non-iterative technique for phase noise ICI mitigation in packet-based OFDM systems," *IEEE Trans. Signal Process.*, vol. 58, pp. 5945–5950, Nov. 2010.

[33] Z. Liu and L. Zhang and Zuwei Chen, "Low PAPR OFDM-based DCSK Design with Carrier Interferometry Spreading Codes," *IEEE Commun. Lett.*, vol. 22, pp. 1588–1591, Aug. 2018.

[34] M. A. Khan and R. K. Rao, "Low-Complexity PAPR Reduction Technique for OFDM Systems Using Biased Subcarriers," *Canadian Journal of Electrical and Computer Engineering*, vol. 39, pp. 19–25, Nov. 2016.